International Journal of Nanoelectronics and Materials
IJNeaM
ISSN 1985-5761 | E-ISSN 2232-1535

The role of solvents on the optical properties of carbon quantum dots synthesized via solvothermal/hydrothermal method

Fani Rahayu Hidayah Rayanisaputri [a], Ferry Anggoro Ardy Nugroho [a], and Vivi Fauzia [a] *

[a]*Departement of Physics, Universitas Indonesia, Depok 16411, Indonesia*
** Corresponding author. E-mail: vivi@sci.ui.ac.id*

Received 17 December 2024, Revised 20 June 2025, Accepted 24 June 2025

ABSTRACT

This research explores how different solvents affect the synthesis and optical properties of carbon quantum dots (CQDs) using a solvothermal method. Previous studies on emission-related applications have emphasized the optical and electrical properties, but there has been little focus on how the choice of solvent affects electrocatalytic applications. The findings demonstrate that the choice of solvent significantly influences the crystallinity, particle size, functional groups, and both absorption and photoluminescence spectra, leading to variations in the band gaps. CQDs-DI had the smallest particles at 3.6 ± 0.6 nm with a polycrystalline structure, CQDs-Glycerol had moderate-sized particles at 6.7 ± 0.6 nm with an amorphous structure, while CQDs-DMF produced the largest particles at 15.1 ± 2.0 nm. FTIR and UV-Vis tests confirmed different functional groups, with CQDs-DMF showing amide groups. The presence of amide groups in CQDs-DMF led to hydrophobic properties, supported by an additional peak in the UV-Vis spectrum at 450 nm, caused by the surface state of C=N. Additionally, TRPL characterization showed that CQDs-Glycerol had the fastest lifetime decay, at 2.3 ns, other than CQDs-DI at 4.73 ns and CQDs-DMF at 5.58 ns. This study demonstrate that DI and glycerol solvent are efficient solvents for synthesizing CQDs as electrocatalysts due to their hydrophilic nature and crystallinity.

Keywords: *Carbon quantum dots (CQDs), Solvothermal, Electrocatalyst, Hydrophobic/hydrophilic functional group*

1. INTRODUCTION

Exploring hydrogen energy as a replacement for fossil fuels is widely recognized as a promising and sustainable solution to meet the growing demand for clean, renewable, and environmentally friendly energy sources [1]. Electrochemical water splitting has emerged as a key approach for producing hydrogen, as it efficiently breaks down water molecules into hydrogen and oxygen through electrocatalysis. This process involves two half-cell reactions: the Oxygen Evolution Reaction (OER) at the anode, where water is oxidized to generate oxygen, and the Hydrogen Evolution Reaction (HER) at the cathode, where hydrogen is produced through the reduction of protons [2, 3]. Currently, noble metals such as platinum (Pt), ruthenium oxide (RuO_2), and iridium oxide (IrO_2) are widely utilized as electrocatalysts for these reactions due to their excellent catalytic performance and stability. However, the scarcity and high cost of these materials present significant barriers to large-scale implementation, thereby driving the search for alternative, cost-effective, and earth-abundant catalysts [4, 5].

In this context, carbon-based materials have emerged as highly promising candidates to enhance the electrocatalytic efficiency of both HER and OER processes [6]. Among these, carbon dots (CDs) have attracted considerable attention due to their unique physicochemical properties, which include nanoscale dimensions, high conductivity, tunable electronic characteristics, and abundant surface functional groups. CDs are generally classified into three main types: carbon nanodots (CNDs), graphene quantum dots (GQDs), and carbon quantum dots (CQDs), with CQDs being the most widely investigated due to their hybrid sp^2/sp^3 carbon structure [6–8]. CQDs are quasi-spherical nanostructures typically smaller than 10 nm, comprising a carbon core surrounded by surface functional groups such as hydroxyl (–OH), carboxyl (–COOH), amine ($–NH_2$), and others. These functional groups not only enhance the solubility and dispersion of CQDs in aqueous and non-aqueous systems but also play a crucial role in modulating their hydrophilicity, charge transport, and interaction with other materials [9–11]. The hydrophilic nature of CQDs, influenced by the presence of polar functional groups [12], allows for better interaction with water molecules during electrocatalytic processes, facilitating efficient electron transfer and improving reaction kinetics. Furthermore, these functional groups provide active sites for catalytic reactions, significantly enhancing their electrocatalytic activity.

The combination of quantum confinement effects and surface functionalities endows CQDs with several notable advantages, including a large surface area for abundant active reaction sites, efficient charge transfer capabilities, and excellent conductivity. These features make CQDs highly suitable for HER and OER, where rapid electron transfer and stable catalytic activity are essential [8, 13].

Additionally, the incorporation of heteroatoms such as nitrogen (N), sulfur (S), phosphorus (P), and boron (B) into the CQD structure significantly influences their electrochemical properties by inducing intramolecular charge redistribution [14, 15]. Doped heteroatoms alter the electronic characteristics of the carbon matrix, creating localized active sites that improve the adsorption and desorption of reactive intermediates during HER and OER processes. Furthermore, heteroatom doping enhances the hydrophilicity of CQDs, promoting better contact with the electrolyte and improving their catalytic efficiency.

Recent studies have demonstrated the exceptional catalytic capabilities of CQDs when integrated with transition metals and their compounds. For instance, in 2019, Feng *et al.* synthesized carbon dots (CDs) via a hydrothermal approach and incorporated them in situ with cobalt (Co) nanoparticles and Co_3O_4 nanostructures. The resulting electrocatalyst exhibited remarkable HER activity, achieving overpotentials of 137 mV and 134 mV at a current density of 10 mA/cm^2 in acidic and alkaline environments, respectively. The study highlighted the role of CDs in controlling the bonding structure between nitrogen-doped carbon (N–C) and Co nanoparticles, as well as facilitating synergistic interactions between the components [16]. Similarly, Song *et al.* (2020) prepared nitrogen-doped CDs through pyrolysis under an argon atmosphere and incorporated them into molybdenum phosphide (MoP), forming MoP/CD composites. The incorporation of nitrogen altered the electronic structure at the active sites, enhancing the HER performance by promoting better hydrogen adsorption, which led to an overpotential of just 70 mV in a 1.0 M potassium hydroxide (KOH) electrolyte at 10 mA/cm^2 [17]. More recently, Dang *et al.* (2022) synthesized nitrogen- and sulphur-co-doped carbon dots (NSCDs) using a plasma-induced method and integrated them with MoS_2/graphene nanosheets to form an NSCD-MoS_2/graphene composite. The combination of zero-dimensional NSCDs with two-dimensional MoS_2/graphene created a high density of edge-active sites, significantly enhancing charge transport and reducing the Tafel slope to 53 mV/dec while achieving a low overpotential of 98 mV at 10 mA/cm^2 [18].

Despite substantial progress in enhancing the electrocatalytic performance of CQDs through surface modification and heteroatom doping, further research is needed to understand the role of synthesis parameters in determining their optical, electrical, and chemical properties. It has been well-documented in emission-related applications that factors such as reaction time, temperature, and solvent choice have a significant impact on the structural and functional characteristics of CQDs, GQDs, and CNDs. For example, Rajender *et al.* (2019) demonstrated that solvents like dimethylformamide (DMF) and dimethyl sulfoxide (DMSO) strongly influence the photoluminescence (PL) spectra of GQDs, primarily by altering surface defect states [19]. Similarly, Tian *et al.* synthesized multi-coloured CDs using citric acid and urea under various solvents and observed that the band gap and optical properties of CDs were affected by the dehydration and carbonization processes, which were solvent-dependent [7]. While these studies provide insights into the optical behaviour of carbon dots, a notable research gap exists regarding the influence of solvents in the solvothermal synthesis of CQDs, GQDs, and CNDs for electrocatalytic applications.

Based on the above discussion, it is imperative to investigate the impact of different solvents used in the one-pot solvothermal synthesis of CQDs on their structural, electronic, and catalytic properties, as well as their hydrophilicity and overall performance in electrochemical and photoelectrochemical water splitting applications. In this study, CQDs were synthesized from citric acid and urea under hydrothermal/solvothermal conditions using three different solvents: deionized water, glycerol, and dimethylformamide (DMF). The choice of solvent significantly influenced the crystallinity, optical properties, and catalytic behaviour of the CQDs. Specifically, CQDs synthesized with DMF (CQDs-DMF) exhibited higher crystallinity and red emission in the PL spectra, whereas those synthesized with deionized water (CQDs-DI) and glycerol (CQDs-Glycerol) displayed polycrystalline structures with blue-emission PL spectra. By investigating the correlation between synthesis parameters, surface functional groups, hydrophilicity, and catalytic performance, this study aims to provide a deeper understanding of the role of CQDs in electrocatalytic water splitting for hydrogen production.

2. EXPERIMENTAL SECTION

Citric acid ($C_6H_8O_7$, 99.5%) and urea (CH_4N_2O, 99%) were purchased from Sigma-Aldrich. N, N-dimethylformamide (DMF, $(CH_3)_2NC(O)H$, 99.8%) was obtained from Loba Chemie, while glycerol ($C_6H_8O_3$, 85%) was purchased from Merck. Deionized (DI) water was used throughout the experiment. A Teflon stainless-steel autoclave was used for hydrothermal/solvothermal reaction.

2.1. Synthesis of CQDs

CQDs were synthesized via a one-pot hydrothermal/ solvothermal method as reported [7] at 160°C for 4 hours, as illustrated in Figure 1. In this process, 3 g of citric acid and 1 g of urea were dissolved in 10 mL of three different solvents (DI water, glycerol, and DMF). The mixture was heated in an autoclave at 160°C for 4 hours, followed by natural cooling to room temperature. The resulting solution was filtered using a 0.22 μm syringe filter and centrifuged at 10,000 rpm for 20 minutes to remove any large unreacted particles. The solutions were labelled as CQDs-DI, CQDs-Glycerol, and CQDs-DMF, and stored at 4°C for further characterization.

2.2. Material Characterization

High-resolution transmission electron microscopy (HRTEM) and FESEM analysis were performed using a TECNAI G2 20 S-TWIN, FEI operated at an accelerating voltage of 200 kV to confirm the morphology and size of the

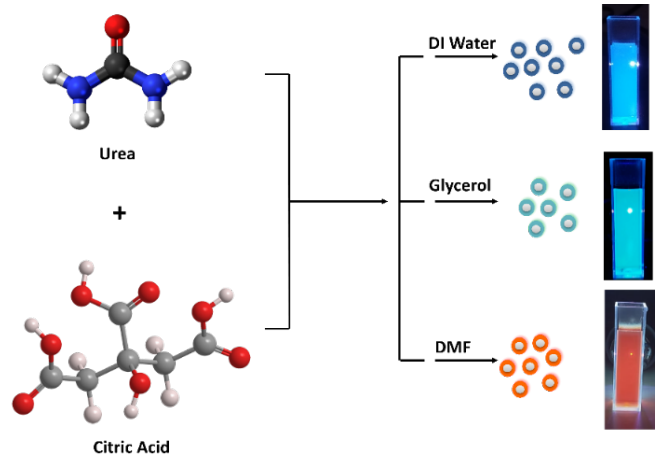

Figure 1. Illustration scheme of synthesized the CQDs using three different solvents (DI, Glycerol, and DMF)

nanoparticles. UV-Vis measurement was carried out using Thermo Scientific UV-Vis spectrophotometer. Photo-luminescence (PL) measurements were performed on an FLS920 Edinburgh instrument with excitation at 325 nm. Thermo Fisher Scientific Nicolet iS50 was used for Fourier transform infrared (FTIR) spectroscopy.

3. RESULTS AND DISCUSSION

3.1. Morphological and Structural Analysis of CQDs

The particle sizes and morphological features of CQDs synthesized with DI water, glycerol, and DMF were analyzed via HRTEM images, lattice fringes, and histogram particle distribution, as shown in Figure 2. Figures 2(a–c) show the TEM imager CQDs-DI, Figures 2(d–f) correspond to CQDs-Glycerol, and Figures 2(g–i) refer to CQDs-DMF. The results indicate significant variations in both the particle size and crystallinity of CQDs based on the solvent used during synthesis. The significant differences in particle size and crystallinity observed among CQDs-DI, CQDs-Glycerol, and CQDs-DMF can be attributed to the solvent properties, particularly their polarity, viscosity, and role in the carbonization process [7].

CQDs synthesized with DI water as shown in Figure 2(a–b), leading to the formation of smaller CQDs with moderately crystalline structures. The moderate polarity of water supports nucleation but does not favour rapid growth, resulting in the smallest average particle size at 3.6 ± 0.6 nm (Figure 2(c)) among the three. CQDs-DI samples show clear

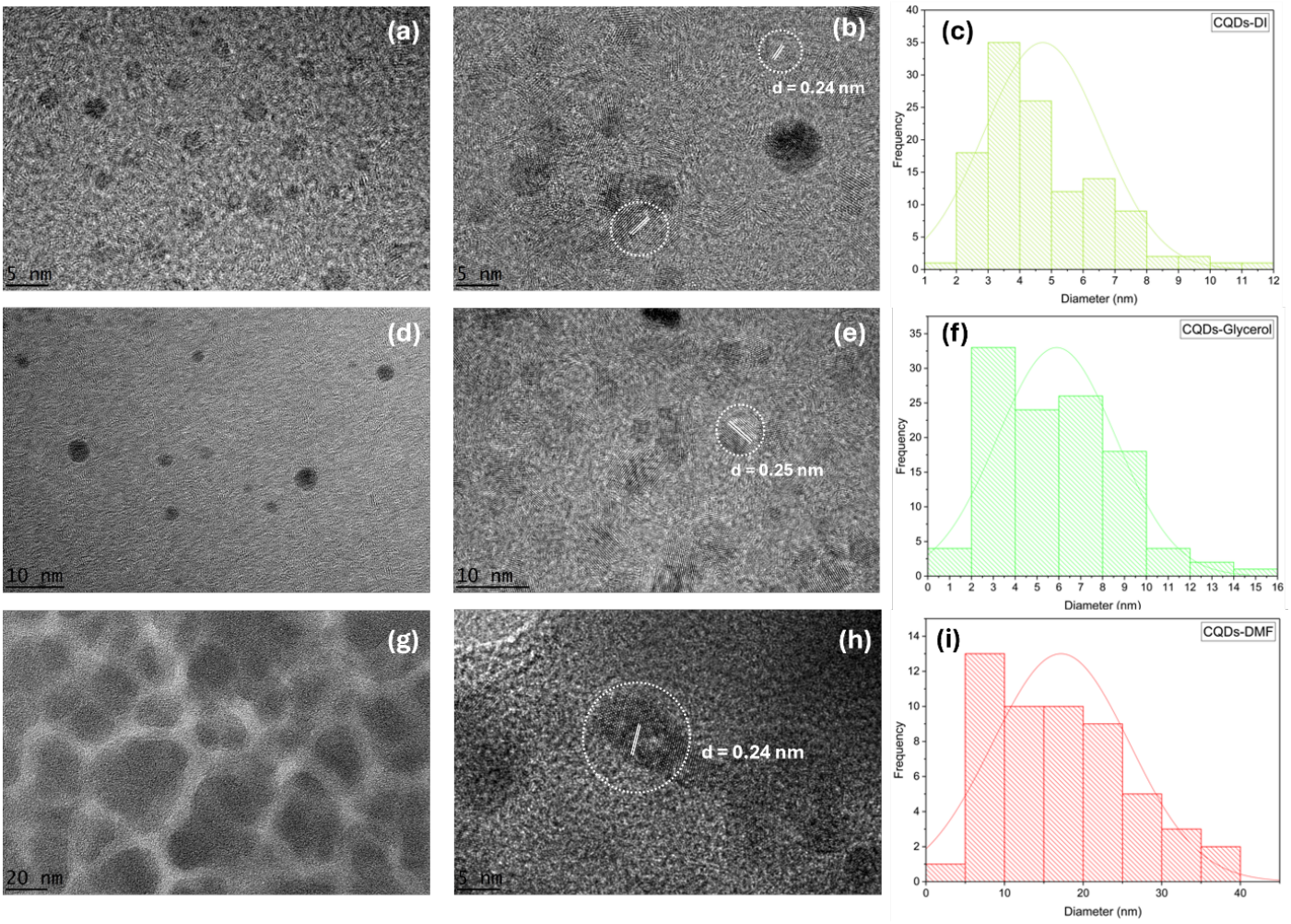

Figure 2. HRTEM images of (a–b) CQDs-DI, (d–e) CQDs-Glycerol, and (g–h) CQDs-DMF. Histogram distribution of the particle size of (c) CQDs-DI, (f) CQDs-Glycerol, and (i) CQDs-DMF

polycrystalline lattice fringes with well-defined and organized patterns. These fringes suggest that CQDs-DI exhibit moderate crystallinity. These fringes suggest that CQDs-DI exhibit moderate crystallinity with interplanar spacing values was 0.24 nm [20–22].

In contrast, CQDs synthesized in glycerol (Figure 2(d–e)), its high viscosity and lower polarity likely slow the rate of nucleation and carbonization [7, 23] , leading to the formation of larger CQDs at 6.7 ± 0.6 nm (Figure 2(f)). However, the slow carbonization process may also result in structural disorder, as evidenced by the amorphous lattice fringes in Figure 2(e). This suggests that while glycerol allows for the growth of larger CQDs, it does not favour the development of highly crystalline structures due to insufficient energy for the alignment of carbon atoms into well-defined lattice planes. The interplanar spacing of CQDs-Glycerol using FFT was measured to be 0.25 nm.

On the other hand, CQDs synthesized in DMF (Figure 2(g–h)) provide that DMF an aprotic and highly polar solvent, provides a more favourable environment for carbonization. Aprotic solvents like DMF, are known to enhance dehydration reactions during the synthesis process, thereby accelerating the conversion of precursors into carbon nuclei and promoting controlled particle growth [24]. The enhanced carbonization efficiency of DMF not only results in larger CQDs (15.1 ± 2.0 nm) but also contributes to their higher degree of crystallinity, as seen in the sharp lattice fringes in Figure 2(h). The interplanar spacing values of CQDs-DMF, determined via FFT patterns using ImageJ software, were measured to be 0.24 nm. These values are consistent with the interlayer spacing of graphitic carbon, further confirming the crystalline nature of CQDs-DMF [25].

The formation mechanism of carbon quantum dots involves the thermal decomposition of citric acid and urea into small organic molecules, followed by polymerization and carbonization processes. During this process, carbon nuclei form and gradually grow into carbon cores, while functional groups such as hydroxyl, carboxyl, and amine groups attach to the CQD surface. The role of the solvent is critical in controlling the nucleation and growth rates of CQDs [22, 26].

3.2. Optical Properties of CQDs

Figure 3(a) displays the UV-Vis absorption spectra of the synthesized CQDs, highlighting distinct optical characteristics based on the solvent used during synthesis. For CQDs-DI and CQDs-Glycerol, strong absorption bands appear in the 200–280 nm and 280–400 nm regions. These bands are attributed to π–π* transitions of C=C bonds and n–π* transitions associated with C=O and C=N bonds, respectively, as reported in previous studies [18, 33–35]. Interestingly, CQDs-DMF exhibit a weak shoulder peak at 454 nm, which is explained by surface state transitions. These transitions arise from electron lone pairs interacting with n–π* transitions, specifically involving C=O and C=N functionalities located at the edges of the carbon structure. Additionally, the extended absorption tail in the visible

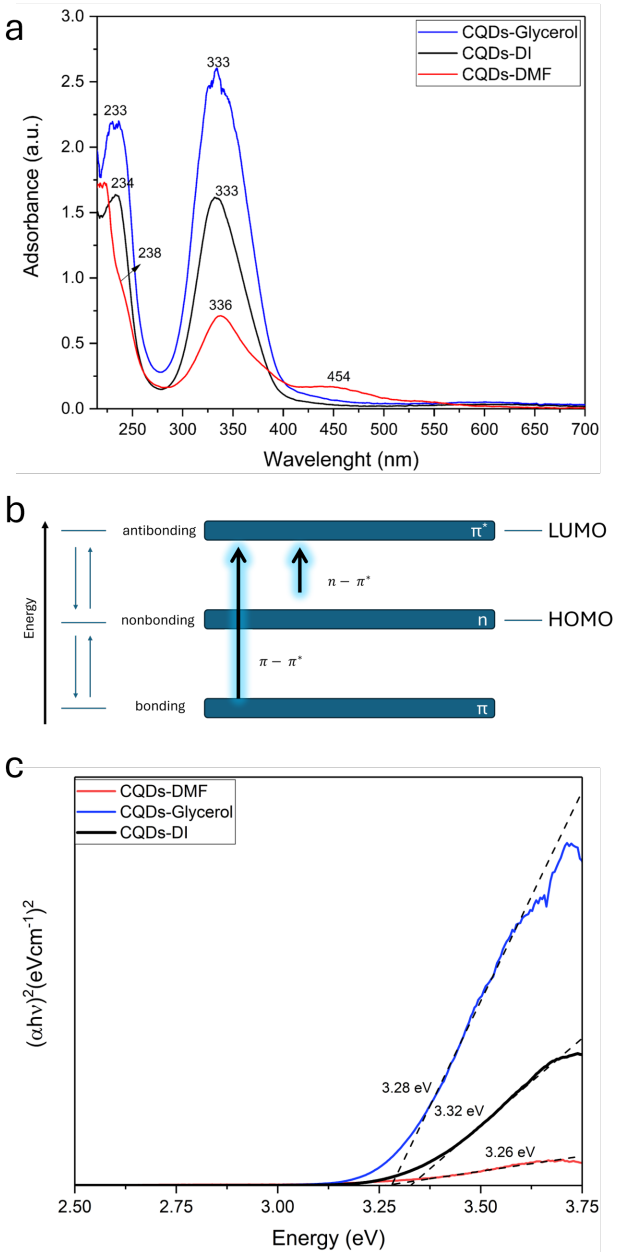

Figure 3. (a) UV-Vis absorbance of CQDs. (b) Illustration diagram energy of CQDs. (c) Tauc plot of CQDs

range for CQDs-DMF is linked to lower-energy surface states introduced by functional groups, such as amino groups [24, 36–38]. Notably, the absorption peak beyond 400 nm is absent in CQDs-DI and CQDs-Glycerol, indicating a distinct solvent-dependent optical response.

Figure 3(b) provides a schematic representation of the electronic transitions (n–π* and π–π*), showcasing the excitation of electrons from the highest occupied molecular orbital (HOMO) to the lowest unoccupied molecular orbital (LUMO). The UV-Vis data suggest that these transitions are most favourable in the synthesized CQDs, correlating with their unique optical properties [33]. Figure 3(c) presents the Tauc plots derived from the UV-Vis spectra, which are used to calculate the band gap energy (Eg) of the CQDs. The band gap was determined using the Tauc relation for direct band gap transitions [34]:

$$\alpha h\nu = C(h\nu - E_g)^n \quad (1)$$

where α represents the absorption coefficient as determined by Beer-Lambert's law, C is a constant, E_g is the band gap energy, and n is $1/2$ for direct band gap transitions [34]. By extending the linear portion of the Tauc plot to the energy axis, the E_g for CQDs-DI, CQDs-Glycerol, and CQDs-DMF were found to be 3.32 eV, 3.28 eV, and 3.26 eV, respectively. These findings reveal that smaller carbon dot sizes correspond to larger band gaps, directly impacting their electronic and photoelectronic behaviour [24].

Figure 4(a) illustrates the appearance of CQD solutions under ambient and UV light (365 nm). Under ambient light, CQDs-DI, CQDs-Glycerol, and CQDs-DMF emit green, yellow, and blue colours, respectively. However, under UV light, the emissions shift, with CQDs-DI and CQDs-Glycerol showing blue-green fluorescence, while CQDs-DMF exhibit a red emission.

Figure 4(b) shows the photoluminescence (PL) spectra of the CQDs at an excitation wavelength of 325 nm. The emission peaks are observed at approximately 469 nm for CQDs-DI, 479 nm for CQDs-Glycerol, and 573 nm for CQDs-DMF. This shift in PL emission suggests a strong correlation between the particle size, shape, and surface chemistry of the CQDs, consistent with previous reports [18].

Time-resolved photoluminescence (TRPL) measurements, also depicted in Figure 4(c), were analysed using a tri-exponential decay model. This analysis revealed multiple radiative and non-radiative recombination pathways in the CQDs. The lifetimes and their respective contributions are summarized in Table 1. These lifetimes are attributed to the recombination of electrons at edge sites and functional group defects in the CQDs [14, 18, 30, 40]. The average decay times (τ_{av}) for CQDs-DI, CQDs-Glycerol, and CQDs-DMF were 4.73 ns, 2.39 ns, and 5.58 ns, respectively. These differences in decay lifetimes highlight how the choice of solvent influences the surface state characteristics of the CQDs [41]. The shorter lifetime of CQDs-Glycerol compared to CQDs-DI and CQDs-DMF suggests a reduced recombination rate, more efficient electron-hole separation, and longer-lived photogenerated electrons [42]. This property is particularly beneficial for applications such as electrochemical water splitting, where prolonged charge separation enhances catalytic performance [18].

In contrast, the longer lifetime observed in CQDs-DMF reflects the influence of surface states that trap charge carriers, thereby delaying recombination. While this could be beneficial for applications requiring long-lived excited states, such as luminescent imaging, it may limit the efficiency of photocatalytic processes.

3.3. Surface Composition of CQDs

The surface functional groups and core structure of CQDs were identified using FTIR spectroscopy. Figure 5 highlights the vibrational modes observed in the spectra. The broad peak in the range of ~3000–3800 cm^{-1} indicates the presence of hydroxyl (C–OH/OH) and amine (NH_2) groups, located both on the in-plane structure and at the edge sites of the CQDs. These functional groups are significant, as they enhance the hydrophilicity of the CQDs, facilitating their dispersibility in polar solvents such as

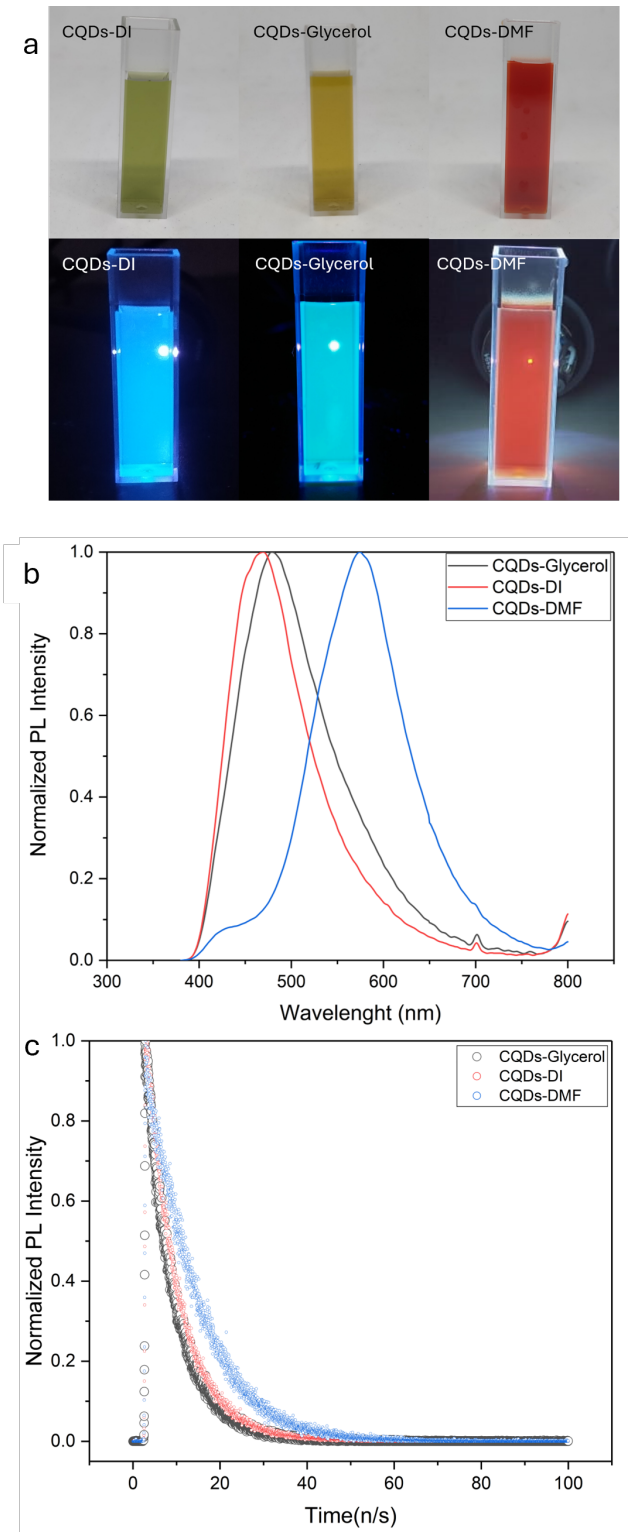

Figure 4. (a) CQDs solution under daylight (top) and UV light 365 nm (bottom). (b) Normalized PL spectra of CQDs. (c) TRPL spectra of CQDs

Table 1. Parameter of the TRPL data for carrier lifetime of the CQDs using three different solvents: DI Water, Glycerol, and DMF

Solvent	Carrier lifetime (τ in ns) and amplitude (B)												
	τ_1	Std dev τ_1	B_1	Std dev B_1	τ_2	Std dev τ_2	B_2	Std dev B_2	τ_3	Std dev τ_3	B_3	Std dev B_3	τ_{av}
DI	0.26	0.01	0.58	0.02	3.41	0.09	0.28	0.01	6.66	1.04	0.15	0.15	4.73
Glycerol	0.20	0.01	0.59	0.02	2.28	0.09	0.25	0.01	4.69	0.44	0.3	0.03	2.39
DMF	0.22	0.01	0.26	0.01	7.19	0.25	0.16	0.01	12.01	1.76	0.2	0.02	5.58
$\tau_{av} = \sum_{i=1}^{3} \frac{B_i \tau_i^2}{B_i \tau_i}$													

water. The vibrational band observed at ~2133 cm^{-1} is attributed to the stretching vibrations of O=C=O groups [27–30]. These carbonyl functional groups are typically found in oxidized carbon materials and are likely to impact the CQDs' ability to interact with other molecules through hydrogen bonding or dipole interactions. Meanwhile, the peak at ~1650 cm^{-1}, present in all samples, is associated with C=C bonds and overlaps with the amide carbonyl stretching vibrations [18, 25]. This indicates the presence of unsaturated carbon as well as amide functionalities, both of which play a role in defining the electronic and chemical characteristics of the CQDs. The peak around 599 cm^{-1} represents C–OH bending vibrations, further confirming the presence of hydroxyl groups [31]. Additional vibrational modes at approximately 1313 cm^{-1} are related to edge oxygen functional groups, including ketones and quinones [18]. A weak vibrational mode observed at ~1460 cm^{-1} in CQDs synthesized using DMF is linked to the in-plane stretching vibrations of sp^2-hybridized carbon atoms (C=C) [6, 18, 21]. The vibrational mode around ~1045 cm^{-1} corresponds to the C–O stretching vibrations, which are commonly associated with alcohols, ethers, or ester groups [25, 26]. This indicates the presence of oxygenated functional groups on the surface of the CQDs. Similarly, the vibrational band around ~1390 cm^{-1} is attributed to C–O epoxy groups attached to the sp^3-hybridized carbon of the CQDs, further corroborating the oxygen-rich nature of the material [21].

The presence of nitrogen functional groups, such as amide N or pyridinic nitrogen, is not sharply evident in the FTIR spectra of CQDs synthesized with DMF. However, the UV-Vis data provide supporting evidence, showing an extended absorption peak in the ~450 nm region. This is attributed to the surface amide groups, which are unique to nitrogen-doped CQDs. This observation points to two distinct types of surface states in the CQDs: (1) oxygenated functional groups, including C=O and C–O, found in all samples, and (2) nitrogenated functional groups, such as C–N–C and C–N–H, which are specific to nitrogen-doped CQDs synthesized with DMF [32].

The functional groups present on the surface of CQDs play a crucial role in determining their hydrophilicity. Hydroxyl (C–OH) and carbonyl (C=O) groups are highly hydrophilic, enabling the CQDs to form hydrogen bonds with water molecules, thereby enhancing their solubility in aqueous environments. Conversely, the presence of nitrogenated

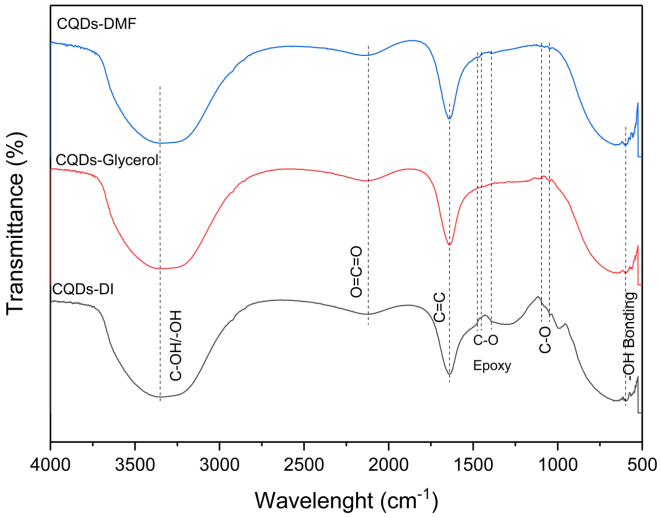

Figure 5. FTIR spectra of CQDs-DI, CQDs-Glycerol and CQDs-DMF

groups, such as pyridinic nitrogen and amide functionalities, can contribute to a more hydrophobic nature due to their reduced polarity compared to oxygenated groups. Epoxy functional groups (C–O) also contribute to the hydrophobicity, especially when present in significant quantities [25]. The balance between these hydrophilic and hydrophobic functional groups determines the overall dispersibility and interfacial properties of the CQDs. This variation in surface chemistry directly impacts their potential applications in aqueous-phase systems, including bioimaging, drug delivery, and photocatalysis.

4. CONCLUSION

This study successfully synthesized carbon quantum dots (CQDs) using three different solvents (DI water, glycerol, and DMF) through the hydrothermal/solvothermal method. The results showed that the solvent affects the particle size, crystallinity, and functional groups of CQDs, which in turn influence their optical and electronic properties. CQDs-DI had a polycrystalline structure with an average particle size of 3.6 ± 0.6 nm, CQDs-glycerol exhibited a more amorphous structure with an average particle size of 6.7 ± 0.6 nm, and CQDs-DMF had the largest size, 15.1 ± 2.0 nm, with higher crystallinity. FTIR and UV-Vis measurements confirmed different functional groups on the CQDs. CQDs-DI and CQDs-Glycerol showed hydroxyl and carbonyl groups, while CQDs-DMF showed the presence of amide groups. The appearance of amide and epoxy groups in CQDs-DMF led to

hydrophobic properties, supported by an additional peak in the UV-Vis spectrum at 450 nm, caused by the surface state of C=N. Additionally, TRPL characterization showed that CQDs-Glycerol had the fastest lifetime decay, at 2.3 ns other than CQDs-DI at 4.73 ns and CQDs-DMF at 5.58 ns. This result shows that DI water and glycerol are efficient solvents for synthesizing CQDs as electrocatalysts due to their hydrophilic nature and crystallinity.

ACKNOWLEDGMENTS

This work was financially supported by Hibah Pendidikan Magister menuju Doktor untuk Sarjana Unggul (PMDSU) NKB-905/UN2.RST/HKP.05.00/2024 from Ministry of research, Technology and Higher Education Republic of Indonesia

REFERENCES

[1] G. Zhao, K. Rui, S. X. Dou, and W. Sun, "Heterostructures for Electrochemical Hydrogen Evolution Reaction: A Review," *Advanced Functional Materials*, vol. 28, no. 43, Oct. 2018, doi: 10.1002/adfm.201803291.

[2] X. Zhang, F. Jia, and S. Song, "Recent advances in structural engineering of molybdenum disulfide for electrocatalytic hydrogen evolution reaction," *Chemical Engineering Journal*, vol. 405, p. 127013, Feb. 2021, doi: 10.1016/j.cej.2020.127013.

[3] X. Zou and Y. Zhang, "Noble metal-free hydrogen evolution catalysts for water splitting," *Chemical Society Reviews*, vol. 44, no. 15, pp. 5148–5180, 2015, doi: 10.1039/C4CS00448E.

[4] G.-L. Li, Y.-Y. Miao, X.-Y. Qiao, T.-Y. Wang, and F. Deng, "Engineering edge sites based on NiS_2/MoS_2/CNTs heterojunction catalyst for overall water splitting," *Applied Surface Science*, vol. 615, p. 156309, Apr. 2023, doi: 10.1016/j.apsusc.2022.156309.

[5] Roger, M. A. Shipman, and M. D. Symes, "Earth-abundant catalysts for electrochemical and photoelectrochemical water splitting," *Nature Reviews Chemistry*, vol. 1, no. 1, p. 0003, Jan. 2017, doi: 10.1038/s41570-016-0003.

[6] F. Yan, Z. Sun, H. Zhang, X. Sun, Y. Jiang, and Z. Bai, "The fluorescence mechanism of carbon dots, and methods for tuning their emission color: a review," *Microchimica Acta*, vol. 186, no. 8, p. 583, Aug. 2019, doi: 10.1007/s00604-019-3688-y.

[7] Z. Tian *et al.*, "Full-Color Inorganic Carbon Dot Phosphors for White-Light-Emitting Diodes," *Advanced Optical Materials*, vol. 5, no. 19, Oct. 2017, doi: 10.1002/adom.201700416.

[8] F. Sher *et al.*, "Carbon quantum dots conjugated with metal hybrid nanoparticles as advanced electrocatalyst for energy applications – A review," *Coordination Chemistry Reviews*, vol. 500, p. 215499, Feb. 2024, doi: 10.1016/j.ccr.2023.215499.

[9] Q. Hou *et al.*, "Application of coal-based carbon dots for photocatalysis and energy storage: a minireview," *New Journal of Chemistry*, vol. 46, no. 36, pp. 17102–17113, 2022, doi: 10.1039/D2NJ03041A.

[10] N. Selvaraju, K. Ravichandran, and G. Venugopal, "A short review of the kinetic parameters of carbon quantum dots for Electrocatalytic Hydrogen evolution reaction," *International Journal of Hydrogen Energy*, vol. 48, no. 10, pp. 3807–3823, Feb. 2023, doi: 10.1016/j.ijhydene.2022.10.203.

[11] S. Zhu, Y. Song, X. Zhao, J. Shao, J. Zhang, and B. Yang, "The photoluminescence mechanism in carbon dots (graphene quantum dots, carbon nanodots, and polymer dots): current state and future perspective," *Nano Research*, vol. 8, no. 2, pp. 355–381, Feb. 2015, doi: 10.1007/s12274-014-0644-3.

[12] H. Yang *et al.*, "Hydrophobic carbon dots with blue dispersed emission and red aggregation-induced emission," *Nature Communications*, vol. 10, no. 1, p. 1789, Apr. 2019, doi: 10.1038/s41467-019-09830-6.

[13] L. Tian, Z. Li, P. Wang, X. Zhai, X. Wang, and T. Li, "Carbon quantum dots for advanced electrocatalysis," *Journal of Energy Chemistry*, vol. 55, pp. 279–294, Apr. 2021, doi: 10.1016/j.jechem.2020.06.057.

[14] J. Cai, X. Zhang, Y. Pan, Y. Kong, and S. Lin, "MoS_2||CoP heterostructure loaded on N, P-doped carbon as an efficient trifunctional catalyst for oxygen reduction, oxygen evolution, and hydrogen evolution reaction," *International Journal of Hydrogen Energy*, vol. 46, no. 69, pp. 34252–34263, Oct. 2021, doi: 10.1016/j.ijhydene.2021.07.220.

[15] M. K. Barman, B. Jana, S. Bhattacharyya, and A. Patra, "Photophysical Properties of Doped Carbon Dots (N, P, and B) and Their Influence on Electron/Hole Transfer in Carbon Dots–Nickel (II) Phthalocyanine Conjugates," *The Journal of Physical Chemistry C*, vol. 118, no. 34, pp. 20034–20041, Aug. 2014, doi: 10.1021/jp507080c.

[16] T. Feng *et al.*, "Morphological and Interfacial Engineering of Cobalt-Based Electrocatalysts by Carbon Dots for Enhanced Water Splitting," *ACS Sustainable Chemistry & Engineering*, vol. 7, no. 7, pp. 7047–7057, Apr. 2019, doi: 10.1021/acssuschemeng.8b06832.

[17] H. Song, Y. Li, L. Shang, Z. Tang, T. Zhang, and S. Lu, "Designed controllable nitrogen-doped carbon-dots-loaded MoP nanoparticles for boosting hydrogen evolution reaction in alkaline medium," *Nano Energy*, vol. 72, p. 104730, Jun. 2020, doi: 10.1016/j.nanoen.2020.104730.

[18] V. D. Dang *et al.*, "Surface-Plasma-Induced One-Pot Synthesis of N,S-Carbon Dot Intercalated MoS_2/Graphene Nanosheets for Highly Efficient Hydrogen Evolution Reaction," *ACS Applied Energy Materials*, vol. 5, no. 10, pp. 12817–12827, Oct. 2022, doi: 10.1021/acsaem.2c02401.

[19] G. Rajender, U. Goswami, and P. K. Giri, "Solvent dependent synthesis of edge-controlled graphene quantum dots with high photoluminescence quantum yield and their application in confocal imaging of cancer cells," *Journal of Colloid and Interface Science*, vol. 541, pp. 387–398, Apr. 2019, doi: 10.1016/j.jcis.2019.01.099.

[20] X. Ma and J. Li, "Preparation of multicolor carbon quantum dots by hydrothermal method and their

functionalization applications," *Journal of Luminescence*, vol. 266, p. 120296, Feb. 2024, doi: 10.1016/j.jlumin.2023.120296.

[21] T. Feng *et al.*, "Color-Tunable Carbon Dots Possessing Solid-State Emission for Full-Color Light-Emitting Diodes Applications," *ACS Photonics*, vol. 5, no. 2, pp. 502–510, Feb. 2018, doi: 10.1021/acsphotonics. 7b01010.

[22] Z. Tian *et al.*, "Full-Color Inorganic Carbon Dot Phosphors for White-Light-Emitting Diodes," *Advanced Optical Materials*, vol. 5, no. 19, Oct. 2017, doi: 10.1002/adom.201700416.

[23] D. Uriarte, C. Domini, and M. Garrido, "New carbon dots based on glycerol and urea and its application in the determination of tetracycline in urine samples," *Talanta*, vol. 201, pp. 143–148, Aug. 2019, doi: 10.1016/j.talanta.2019.04.001.

[24] D. Ozyurt, M. al Kobaisi, R. K. Hocking, and B. Fox, "Properties, synthesis, and applications of carbon dots: A review," *Carbon Trends*, vol. 12, p. 100276, Sep. 2023, doi: 10.1016/j.cartre.2023.100276.

[25] S. Kim *et al.*, "Anomalous Behaviors of Visible Luminescence from Graphene Quantum Dots: Interplay between Size and Shape," *ACS Nano*, vol. 6, no. 9, pp. 8203–8208, Sep. 2012, doi: 10.1021/nn302878r.

[26] Z. He *et al.*, "Recent advances of solvent-engineered carbon dots: A review," *Carbon*, vol. 204, pp. 76–93, Feb. 2023, doi: 10.1016/j.carbon.2022.12.052.

[27] P. Roy, P.-C. Chen, A. P. Periasamy, Y.-N. Chen, and H.-T. Chang, "Photoluminescent carbon nanodots: synthesis, physicochemical properties and analytical applications," *Materials Today*, vol. 18, no. 8, pp. 447–458, Oct. 2015, doi: 10.1016/j.mattod.2015.04.005.

[28] P. Kumar, S. Dua, R. Kaur, M. Kumar, and G. Bhatt, "A review on advancements in carbon quantum dots and their application in photovoltaics," *RSC Advances*, vol. 12, no. 8, pp. 4714–4759, 2022, doi: 10.1039/ D1RA08452F.

[29] T. Balakrishnan, W. L. Ang, E. Mahmoudi, A. W. Mohammad, and N. S. Sambudi, "Formation mechanism and application potential of carbon dots synthesized from palm kernel shell via microwave assisted method," *Carbon Resources Conversion*, vol. 5, no. 2, pp. 150–166, Jun. 2022, doi: 10.1016/j.crcon. 2022.01.003.

[30] M. Liu, "Optical Properties of Carbon Dots: A Review," *Nanoarchitectonics*, vol. 1, no. 1, pp. 1–12, Jan. 2020, doi: 10.37256/nat.112020124.1-12.

[31] M. Ali, A. S. Anjum, A. Bibi, S. Wageh, K. C. Sun, and S. H. Jeong, "Gradient heating-induced bi-phase synthesis of carbon quantum dots (CQDs) on graphene-coated carbon cloth for efficient photoelectrocatalysis," *Carbon*, vol. 196, pp. 649–662, Aug. 2022, doi: 10.1016/j.carbon.2022.05.040.

[32] P. Kumar, S. Dua, R. Kaur, M. Kumar, and G. Bhatt, "A review on advancements in carbon quantum dots and their application in photovoltaics," *RSC Advances*, vol. 12, no. 8, pp. 4714–4759, 2022, doi: 10.1039/ D1RA08452F.

[33] K. J. Mintz *et al.*, "A deep investigation into the structure of carbon dots," *Carbon*, vol. 173, pp. 433–447, Mar. 2021, doi: 10.1016/j.carbon.2020.11.017.

[34] Y. Yang *et al.*, "Fluorescent N-Doped Carbon Dots as *in Vitro* and *in Vivo* Nanothermometer," *ACS Applied Materials & Interfaces*, vol. 7, no. 49, pp. 27324–27330, Dec. 2015, doi: 10.1021/acsami.5b08782.

[35] M. Choppadandi *et al.*, "Structural features regulated photoluminescence intensity and cell internalization of carbon and graphene quantum dots for bioimaging," *Materials Science and Engineering: C*, vol. 129, p. 112366, Oct. 2021, doi: 10.1016/j.msec. 2021.112366.

[36] R. L. Calabro, D.-S. Yang, and D. Y. Kim, "Controlled Nitrogen Doping of Graphene Quantum Dots through Laser Ablation in Aqueous Solutions for Photoluminescence and Electrocatalytic Applications," *ACS Applied Nano Materials*, vol. 2, no. 11, pp. 6948–6959, Nov. 2019, doi: 10.1021/acsanm. 9b01433.

[37] M. Ali, A. S. Anjum, R. Riaz, A. Bibi, K. C. Sun, and S. H. Jeong, "Unraveling the surface states related Stokes shift dependent electrocatalytic activity of N-doped carbon quantum dots for photovoltaic applications," *Carbon*, vol. 181, pp. 155–168, Aug. 2021, doi: 10.1016/j.carbon.2021.04.075.

[38] S. Qiu *et al.*, "Carbon dots decorated ultrathin CdS nanosheets enabling in-situ anchored Pt single atoms: A highly efficient solar-driven photocatalyst for hydrogen evolution," *Applied Catalysis B: Environmental*, vol. 259, p. 118036, Dec. 2019, doi: 10.1016/j.apcatb.2019.118036.